Chemical Engineering Science 66 (2011) 6525–6535

Contents lists available at SciVerse ScienceDirect

Chemical Engineering Science

journal homepage: www.elsevier.com/locate/ces

# Using H-titanate nanofiber catalysts for water disinfection: Understanding and modelling of the inactivation kinetics and mechanisms

Meng Nan Chong [a,b,c], Bo Jin [b,c,*], Christopher P. Saint [d]

[a] CSIRO Land and Water, Ecosciences Precinct, Dutton Park Queensland 4102, Australia
[b] School of Chemical Engineering, The University of Adelaide, Adelaide 5005, South Australia
[c] School of Earth and Environmental Sciences, The University of Adelaide, Adelaide 5005, South Australia
[d] SA Water Centre for Water Management and Re-use, University of South Australia, Mawson Lakes 5095, South, Australia

ARTICLE INFO

*Article history:*
Received 27 July 2011
Received in revised form
8 September 2011
Accepted 11 September 2011
Available online 17 September 2011

*Keywords:*
Catalysis
Kinetics
Mathematical modelling
Nanostructure
Photocatalysis
Titanium dioxide

ABSTRACT

The H-titanate nanofiber catalyst (TNC), which has a favourable morphological structure for mass transfer and energy access, was proven as a promising alternate titanium dioxide ($TiO_2$) carrier for photo-inactivation of a sewage isolated *E. coli* strain (ATCC 11775). This study revealed that the TNC loading is a key process parameter that radically influenced the photo-inactivation of bacteria in an annular slurry photoreactor (ASP) system. Variation in the TNC loadings was found to have a considerable impact on the dissolved oxygen (DO) concentration profiles and subsequently, on the photo-inactivation rates of bacteria in the ASP system. The photo-inactivation reaction in the ASP system was found to exhibit three different bacterial inactivation regimes of shoulder, log-linear and tailing. Resultant photo-inactivation kinetics data was evaluated using both empirical and mechanistic bacterial inactivation models. The modified Hom model was found to be the best empirical model that can represent the sigmoid-type bacterial inactivation pattern. An interesting correlation between the TNC loadings and DO concentration profiles was also established. From the correlation, it was found necessary to integrate a DO limiting reactant term in the newly proposed mechanistic Langmuir–Hinshelwood model to describe the bacterial inactivation mechanisms under two different TNC loading conditions of sub-optimal and optimal, respectively.

© 2011 Elsevier Ltd. All rights reserved.

## 1. Introduction

The presence of microbial contaminants, such as pathogens in water sources that are intended for either potable or indirect potable uses is of major concern owing to the potential implicated human health and environmental risks (WHO, 1997). To date, chlorination is widely used as the most effective disinfection method to remove microbial contaminants from water sources as well as maintaining a residual free chlorine concentration to suppress further microbial regrowth (Vogt and Regli, 1981; Bull et al., 1990; Smith and Rose, 1998; Carter et al., 2000). Recently, the use of chlorination has come under close scrutiny due to the co-formation of disinfection by-products (DBPs) such as trihalomethanes (THMs) and haloacetic acids (HAAs). These DBPs are highly toxic and can cause significant risks to the environment and public health, owing to their promotion of congenital cardiac defects and carcinogenic properties (Marugán et al., 2008; Coleman et al., 2005; US EPA, 2001). The current US EPA allowable limits for regulated DBPs are 80 and 60 ppb for THMs and five HAAs in the treated water, respectively (US EPA, 2001; Coleman et al., 2005). However, it was reported that there are an abundance of other non-regulated DBPs that are also conveying similar deleterious effects and risk consequences (US EPA, 2001; Coleman et al., 2005).

Considering all these issues, clean water treatment technologies that can simultaneously disinfect microorganisms and further prevent the formation of DBPs are of increasing interest. Among the clean water treatment technologies, heterogeneous photocatalysis utilising semiconductor titanium dioxide ($TiO_2$) is an attractive and promising disinfection method to replace the conventional chlorination method (Gamage and Zhang, 2010; McCullagh et al., 2006; Foster et al., 2011). Reactive oxygen species (ROS) (i.e. $OH^{\bullet}$, $O_2^{\bullet -}$ and $H_2O_2$) generated from the photo-induced $TiO_2$ surface charge separation have a high oxidation capacity to mineralise organic contaminants and disinfect microorganisms in water (Cho et al., 2004; Rincón and Pulgarin, 2003, 2004). These ROS are usually short-lived, unselective and react instantaneously with organic and microbial contaminants, leading to their complete removal from water sources (Maness et al., 1999).

* Corresponding author at. School of Earth and Environmental Sciences, The University of Adelaide, Adelaide 5005, South Australia. Tel.: +61 8 8303 7056; fax: +61 8 8303 6222.
*E-mail address:* bo.jin@adelaide.edu.au (B. Jin).

0009-2509/$ - see front matter © 2011 Elsevier Ltd. All rights reserved.
doi:10.1016/j.ces.2011.09.020

Other advantages of $TiO_2$ photocatalysis treatment include chemical-free disinfection and no formation of secondary contaminants such as DBPs. Thus, $TiO_2$ photocatalysis is an ideal clean disinfection technology for water and wastewater treatment. Vidal et al. (1999) estimated that using a tertiary photocatalytic disinfection treatment can provide a competitive treatment cost of \$0.70/$m^3$ of treated water, which is still relatively high when compared to the chlorination cost of \$0.10/$m^3$ of treated water (Burch and Thomas, 1998; Vidal et al., 1999). However, the use of $TiO_2$ photocatalysis treatment is highly sustainable and prevents DBPs formation in the treated water. Significant reduction in photocatalysis treatment cost is foreseeable in the future given the current progress in the research and development works.

At present, the application of $TiO_2$ photocatalysis for disinfection is still being impeded by the post-separation and recovery of fine $TiO_2$ particles after water treatment (Vidal et al., 1999). In this instance, the fine $TiO_2$ particles can still remain in the treated water could present a potentially toxic threat to consumers of treated drinking water. A number of studies have attempted to develop better-engineered $TiO_2$ photocatalysts with comparable oxidation capacity, while presenting a physical macrostructure for ease of particle separation and recovery after water treatment. This includes immobilisation of nano-sized $TiO_2$ particles onto inert substrates such as clay minerals, fibre optics and magnetic cores (Vidal et al., 1999; Chong et al., 2010a). However, the immobilised photocatalysts usually have a lower oxidation capacity due to their structurally impeded light photon path, increased tortuosity within the physical macrostructure of the catalyst and mass transfer resistance that all prohibit rapid mass transfer between reactants and substrates (Vidal et al., 1999; Chong et al., 2009a). Previously, a novel H-titanate nanofiber catalyst (TNC) with thin and long fibril morphology was developed to resolve the post separation, recovery and impracticality in applying Degussa P-25 $TiO_2$ photocatalyst for water disinfection purposes (Zhu et al., 2004, 2005). TNC consists of small anatase $TiO_2$ crystals of 10–20 nm deposited onto titanate fibrils of 40–100 nm thickness and length up to 30 μm. The photoactivity of TNC for removal of organic contaminants was previously investigated (Chong et al., 2009b, 2010c). The major advantages of using TNC include low mass transfer resistance due to its thin fibril morphology, ease of particle dispersion and recovery by free particle settling (Chong et al., 2009b).

Preliminary studies on $TiO_2$ photocatalysis for water disinfection have been demonstrated on a range of coliforms, viruses, bacteria, cysts, fungi, algae and protozoa (Watts et al., 1994; Wolfrum et al., 2002; Hong and Otaki, 2003; Ibánez et al., 2003; Sun et al., 2003). Most of these studies were carried out to investigate different process operational parameters such as light source, catalyst loading and pH on photo-inactivation of microbial contaminants. Surprisingly, after Matsunaga et al.'s (1985) pioneering work on the bactericidal effect of semiconductor $TiO_2$, very few studies have focused on the mechanistic description and kinetic modelling of microbial inactivation during water treatment (Dalrymple et al., 2010). Mostly, the previous photo-disinfection kinetic studies found in the literature were fitted using empirical models. To date, the most commonly used kinetic expression is the classical Chick–Watson (CW) model with different *CT* values for comparison of disinfection efficiency purposes (Cho et al., 2003; Lambert et al., 1999; Lambert and Johnston, 2000). The understanding of photo-inactivation kinetics and mechanisms are of significant importance for design, optimisation and operation of large-scale photocatalytic water treatment processes (Dalrymple et al., 2010). To date, most of the reported studies on photocatalytic disinfection treatment were carried out in a laboratory scale system using Degussa P-25 $TiO_2$ photocatalyst. Process development using a practically feasible photocatalyst and improvement of knowledge on photo-inactivation kinetics and mechanisms are the essential steps toward commercialisation of photocatalytic disinfection treatment technology in the near future.

In this study, the TNC was assessed for its photo-inactivation performance on the bacterium *E. coli* in an annular slurry photoreactor (ASP) system. A sewage-isolated *E. coli* strain ATCC 11775 was used as an indicator microorganism for faecal contamination and microbiological standard to measure against the photo-inactivation efficiency of TNC. The purpose of using the wastewater isolated *E. coli* strain over other common laboratory strains is to permit measurement of disinfection ability against an environmental isolate rather than a possibly attenuated laboratory strain that may yields misleading results (Chong et al., 2011). So far, *E. coli* is the most widely used standard microbial contaminant in water disinfection studies (Dunlop et al., 2002; Coleman et al., 2005). Previously, we have studied the bacterial inactivation kinetics under different effects of TNC loadings, pH, dissolved oxygen (DO) and bacterial inoculum size as well as the associated residual disinfecting effect of TNC (Chong et al., 2010b). However, the emphasis of this study is on how different TNC loadings can influence the bacterial inactivation kinetics and DO concentration profiles during the photo-inactivation reactions in an ASP system. Resultant experimental data will be evaluated using different empirical bacterial inactivation models. The kinetic parameters obtained from the fitting of empirical models will be compared to DO-correlated mechanistic models, which functionalise on the TNC loading conditions. Cross-validation

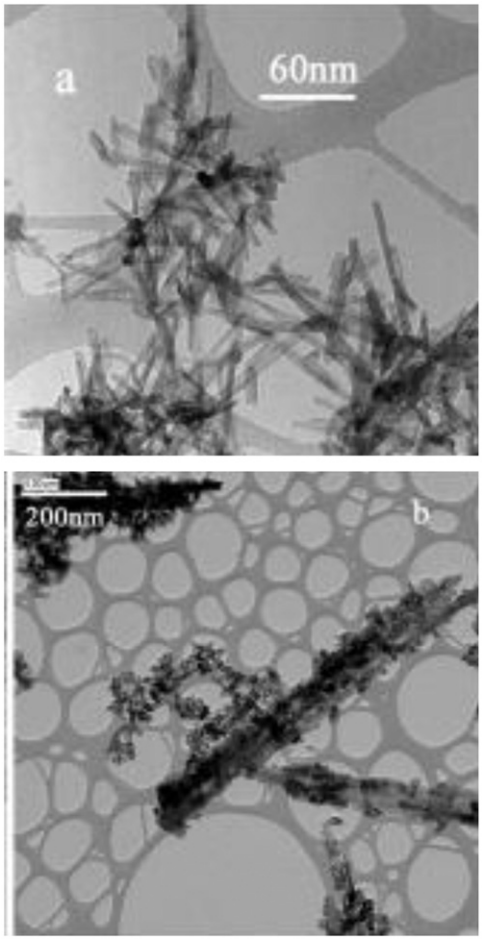


**Fig. 1.** TEM images of H-titanate nanofibers. (a) At 60 nm magnification. (b) At 200 nm magnification.

experiments will also be conducted to verify the robustness of proposed mechanistic models on the photo-inactivation of *E. coli* in a TNC–ASP system.

## 2. Material and methods

### 2.1. Materials

TNC was synthesised through a hydrothermal reaction between concentrated NaOH and $TiO_2$, and a post-synthesis ion-exchange with HCl solution (Zhu et al., 2004, 2005). Specifically, 3 g of anatase particles (~325 mesh from Sigma-Aldrich) was mixed with 80 mL of 10 M NaOH. The resultant suspension was sonicated for 30 min and transferred into a PTFE container for autoclaving. The autoclave was maintained at a hydrothermal temperature of 180 °C for 48 h. The precipitate (sodium titanate nanofibers) was recovered, washed with distilled water (to remove excess NaOH) and finally exchanged with $H^+$ (using a 0.1 M HCl solution) to produce TNC. This was repeatedly washed with distilled water until pH 7 was reached. The hydrogen titanate product was dried at 80 °C for 12 h and further calcined at 700 °C for 3 h to yield TNC. Fig. 1 shows the transmission electron microscopy (TEM) images for the synthesised TNC. The TNC has a dimension of 40–100 nm thickness and length up to 30 μm, on which 10–20 nm anatase $TiO_2$ crystals were deposited. Further detailed synthesis and microscopic characterisations of TNC can be obtained from Zhu et al.'s (2004, (2005) works.

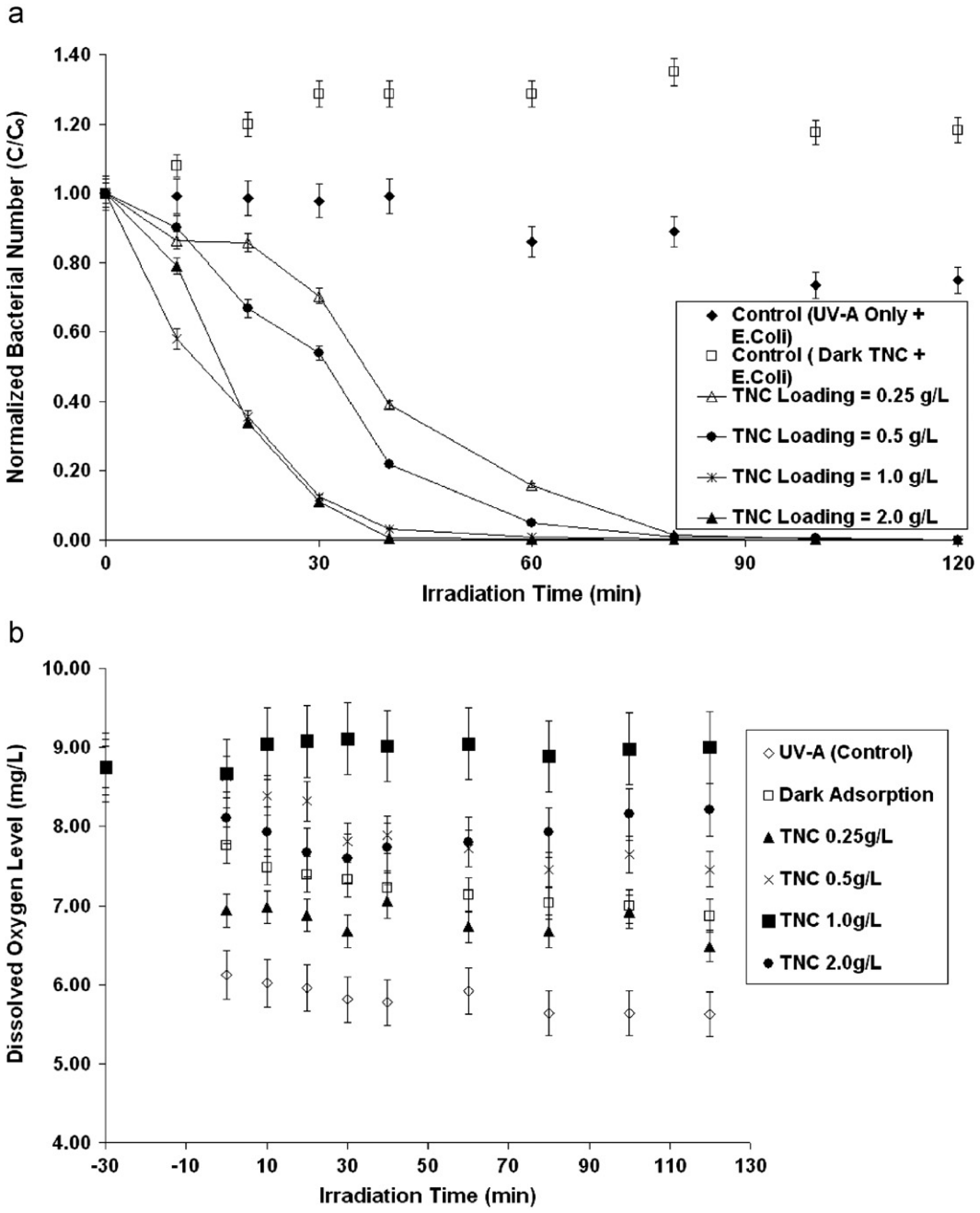


**Fig. 2.** Photocatalytic inactivation of aqueous *E. coli* (ATCC 11775) suspension of average initial density $7 \times 10^6$ CFU $mL^{-1}$. (a) Bacterial reduction ratio ($N/N_o$) against irradiation time (reproduced from Chong et al., 2010b). (b) Measured DO profiles UVA irradiation starts at irradiation time, $t=0$ min.

The TNC can be easily separated by physical sedimentation and is of great significance for application in commercial scale water and wastewater disinfection treatment.

### 2.2. Annular photocatalytic reactor system

A recently developed stainless steel-lined ASP system was used in this study (Chong et al., 2009b). The ASP was operated as a 3-phase continuous air-aerated open system, where TNC was dispersed in the targeted water for photocatalytic disinfection treatment. The lower-end of the ASP was fabricated with a detachable conical bottom to prevent a reaction dead zone, and making it easy for periodic cleaning and maintenance. A 45-μm air sparger was fitted to the bottom to provide homogeneous bubble distribution for agitation, mixing and aeration purposes. The light positioning in the ASP was designed in such a way to permit additional light to be placed within the central quartz tube. An 8 W UVA black light (NEC, Holland) was placed within the quartz thimble to prevent direct contact with reaction water, while allowing optimal UV transmission for the photonic activation of TNC. It should be stressed that the use of UVA light was purely for photonic surface activation of TNC. Unlike germicidal UVC light with high-end UV electromagnetic spectrum (i.e. 4.43–12.4 eV), the associated lethal dose for UVA is significantly lower (i.e. 3.10–3.94 eV) and will not cause substantial bacterial inactivation (Rincón and Pulgarin, 2006). The lamp simulates the UVA component of solar radiation (315–400 nm). Samples were collected from the four-levelled sampling ports on ASP. Electronic probes and metres for in-situ data logging of pH, DO and temperature (TPS, Australia) were connected to the ASP. The operating temperature was kept at 25 °C during experiments. Previously, we have detailed a schematic for the ASP system and the whole experimental set up (Chong et al., 2009b).

### 2.3. Photocatalytic disinfection experiments

During the batch study, the ASP was filled with 1.5 L of bacterial suspension at a given bacterial cell density. Fifty-mL of fresh liquid culture was prepared in tryptone soy broth medium (TSB) (Oxoid, England) and incubated in a rotary shaker at 150 rpm and 35 °C for 19 h. The final bacterial cell density was determined to be $9\times10^9$ CFU $mL^{-1}$.

For the bacterial suspension, an aliquot of the incubated liquid culture was directly inoculated into 1.5 L of phosphate buffered saline (PBS) solution that was prepared using Nanopure Water of 18.2 MΩ cm resistivity. The use of PBS is to prevent sudden osmotic shock to the bacteria, so as to maintain the bacterial numbers for accurate dilution purposes (Chong et al., 2010b, 2011). Subsequently, the initial bacterial density was determined via the heterotrophic plate counting (HPC) method.

During the batch disinfection study, a fixed amount of TNC was added to the *E. coli* suspension and further homogenised in the dark for 30 min under constant aeration. A 5 L/min aeration rate was used as determined from the previous optimisation study (Chong et al., 2010b). After the homogenisation period, UVA light was turned on at $t=0$ min and run continuously for up to 120 min. Samples were collected every 10 min up to 40 min, and thereafter every 20 min up to 120 min. Enumeration of the *E. coli* was carried out by following a standard serial dilution procedure and every sample was subjected to HPC on the plate count agar (PCA) (Merck, Germany) in triplicate. The PCA plates were incubated at 35 °C for 24 h before final cell counting. Normalised fraction of bacterial survivors against irradiation time was plotted for bacterial inactivation analysis. The batch experiments were repeated for standard experimental verification and error analysis.

## 3. Results and discussion

### 3.1. Impact of TNC loadings on dissolved oxygen profiles

The effects of photocatalyst loading on bacterial inactivation rate have been extensively studied using different semiconductor photocatalytic systems (Coleman et al., 2005; Cho et al., 2004). Fig. 2a shows the *E. coli* inactivation profiles under different TNC loadings of 0.25–2.0 g/L (Chong et al., 2010b). Since DO is a primary reactant in the photocatalysis reaction, as well as to support the bacterial respiration activity in the ASP system, a standard DO electrode was used to verify which bacterial activity will pre-dominant on DO during the photo-inactivation reactions (Rincón and Pulgarin, 2005).

Fig. 2a shows that no substantial bacterial inactivation took place under the following control condition: (1) the absence of TNC (UVA+*E. coli*), and (2) absence of UV irradiation (dark TNC +*E. coli*) experiments. However, the *E. coli* concentration reduced significantly (i.e. one-log bacterial reduction) within the first 40 min of UVA irradiation when TNC was added (Chong et al., 2010b). When TNC loading increased from 0.25 to 1.0 g/L, the photo-inactivation rate increased significantly. A plateau in the photo-inactivation rate was observed when the TNC loading was doubled from 1.0 to 2.0 g/L (Chong et al., 2010b). It was observed that 120 min of irradiation was required to achieve a 5-log bacterial reduction at TNC loading of 0.25 g/L (Chong et al., 2010b).

Simultaneous change in DO concentration profile at TNC loading of 0.25 g/L was found to be less significant than both the control experiments. This might be owing to the open ASP system being continuously aerated during the photo-inactivation reaction. Fig. 2b shows that the control experiment with UVA+*E. coli* consumed less DO for bacterial respiration activity, while substantial DO consumption was evidenced in the dark+TNC+*E. coli* control experiment for bacterial growth. In this instance, the direct UVA energy absorption by light sensitive cellular components in *E. coli* creates an intermittent destructive effect on the cell itself without causing a complete inactivation (Rincón and Pulgarin, 2005). Bacterial growth consumed a substantial amount of DO, as evidenced from the low DO consumption rate in the control experiment without UVA irradiation. The low *E. coli* inactivation rate at 0.25 g/L was explained by the partially intercepted DO utilisation rate in the dark and thus, the competition for DO directly resulted in a lower ROS generation rate.

When the TNC loading increased to 0.5 g/L, a shorter irradiation time of 100 min was required to achieve a 5-log bacterial reduction. In this instance, the relative DO concentration decay was considerably less than that of 0.25 g/L TNC loading. In this instance, the increase in photo-inactivation rate was proportional to the doubling in TNC loading from 0.25 to 0.5 g/L. The doubling in TNC loading led to a higher photo-inactivation rate. The DO concentration decay profile was found to shift upward and closer to the DO saturation value than that of 0.25 g/L of TNC loading. In this case, the smaller decay in DO concentration profile was deduced to be offset by the simultaneous release of intracellular trapped oxygen and rapid DO replenishment from the air-water equilibrium. Thus, it can be concluded that the higher DO concentration profile associated with 0.5 g TNC /L loading was mainly dominated by the ROS generation rate.

Fig. 2a shows that the doubling in TNC loading from 1.0 to 2.0 g/L resulted in a plateau in the photo-inactivation rate required to achieve a 5-log bacterial reduction. This showed that the optimal TNC loading in the ASP was 1.0 g/L. At the optimal TNC loading, it was interesting to note that the DO concentration decay profile was rapidly rejuvenated (~8.75 mg/L) within the first 30 min of reaction and remained close to the DO saturation

value for the rest of the photo-inactivation reaction on *E. coli*. Such a trend in DO profile can be explained by the possibly optimal dispersion of illuminated TNC active sites where a maximal number of ROS was generated for the photo-inactivation reaction. This finding was further supported by the length of the shoulder characteristic region in the bacterial survivor curve, where the shortest shoulder and rapid log-linear bacterial reduction characteristics were in evidence. Marugán et al. (2008) reported that the length of the shoulder region was due to the volumetric ROS generation rate, which is a factor of photocatalyst concentration and incident radiation flow within the reactor. Our results revealed that the DO decay mechanism was influenced by the rapid volumetric ROS generation rate rather than the slower DO uptake rate for bacterial respiration activity. The variation in DO profiles indicated that the optimal TNC loading at 1.0 g/L appeared to have insignificant impact on the overall mass transfer during the photocatalysis reaction. Fig. 2b exhibits that the DO was a non-limiting reactant for the photo-inactivation of *E. coli* at optimal TNC loading. Thus, it can be concluded that different TNC loadings have a direct impact on the DO concentration profiles and the eventual photo-inactivation rate of *E. coli*. Cho et al. (2004) also concluded such a relationship between DO and the rate of photoactivity in $TiO_2$. This relationship should be particularly noted during the development of a mechanistic bacterial inactivation model.

### 3.2. Evaluation and modelling of photo-inactivation kinetics

This study revealed that the classical CW model appeared to be inadequate for explaining the photo-inactivation kinetics and mechanisms in the TNC–ASP system. Unlike other photocatalysts, the photo-inactivation reaction in the TNC–ASP system resulted in three different bacterial inactivation regimes. The bacterial inactivation profiles began with (i) a lag or initial smooth decay, known as "shoulder", followed by (ii) a typical log-linear inactivation region and ends with (iii) a long deceleration process, which is known as the "tail" (Chong et al., 2011). The presence of a shoulder characteristic region was justified by the nature of the cumulative damage effect caused by photocatalytic action on the cytoplasmic membrane rather than an instantly lethal affect (Gyürék and Finch, 1998). This can also be viewed in terms of the slow permeation rate of ROS species through the bacterial cell-wall, which were bounded by their short half-life before inducing an irreversible damage to the bacterial cells (Chong et al., 2010a). The tail characteristic, however, is not well-understood. Benabbou et al. (2007) proposed that the tail characteristic region can prolong the entire disinfection treatment process. This was caused by the competition between organic products released from constant cell lyses and the remaining intact cells. Others proposed that the tailing deviation from conventional log-linear bacterial survivor curves was due to the presence of variants in the bacterial population resistant to the disinfection method used (Lambert and Johnston, 2000).

For the empirical models, a demand-free condition was assumed where the photocatalyst loadings during the irradiation period were considered to be constant. To compare the photo-inactivation activity on *E. coli* in the TNC–ASP system, we fitted the experimental data with different empirical models so as to obtain the kinetic parameters. Hom (1972) reproduced a useful empirical integration of the CW model after having observed a curvilinear disinfection plot, rather than the typical log-linear type (Eq. (1));

$$\log \frac{N}{N_o} = -kC^n T^m \tag{1}$$

where $\log(N/N_o)$ is the bacterial log reduction; $N$ is the number of bacterial survivors at irradiation time $t$; $k$ is the experimental reaction rate; $C$ is the concentration of photocatalyst used; and $m$ and $n$ are the empirical constants.

The Hom model is a two-parameter empirical inactivation model that can either represent the shoulder or tail characteristic region. A further modification to the Hom model was proposed, in order to reproduce different inactivation regions during the photo-inactivation reaction (Marugán et al., 2008; Cho et al., 2003; Chong et al., 2011). This modified Hom model (Eq. (2)) expands the applicability of original Hom model for simultaneous fitting of shoulder, log-linear reduction and tailing characteristic regions:

$$\log \frac{N}{N_o} = -k_1\left[1-\exp(-k_2 t]^{k_3}\right. \tag{2}$$

where $k_1$, $k_2$ and $k_3$ are the empirical constants for the modified Hom model representing the shoulder, log-linear reduction and tailing characteristic regions, respectively.

Another empirical model that can represent the different regions found in the photo-inactivation kinetics of bacteria is the power law expression (Eq. (3)), where $x$ and $n$ are the empirical power law constants (Gyürék and Finch, 1998; Chong et al., 2011):

$$\frac{dN}{dt} = -kN^x C^n \tag{3}$$

Integration of this power rate law yields the Rational model (Eq. (4))

$$\log \frac{N}{N_O} = -\frac{\log[1+N_o^{x-1}(x-1)kC^n T]}{(x-1)} \tag{4}$$

The Rational model (Eq. (4)) can represent both the shoulder and tailing characteristics when $x$ is less than or greater than unity, respectively. Similarly, the Hom model (Eq. (1)) can also be integrated accordingly to yield a four-parameter Hom-Power law model (Eq. (5)) (Anotai, 1996; Chong et al., 2011)

$$\log \frac{N}{N_O} = -\frac{\log[1+N_o^{x-1}(x-1)kC^n T^m]}{(x-1)} \tag{5}$$

The Selleck model (Eq. (6)) was also evaluated, since it reduced the number of null parameters in the empirical model (Gyürék and Finch, 1998)

$$\frac{dS}{dt} = \frac{kCS}{1+KCT} \tag{6}$$

where $S$ is the survival ratio$=N/N_o$ at irradiation time $t$; $k$ and $K$ are the rate constants. This Selleck expression accounts for the occurrence of a shoulder region, as it resembles the mechanistic Langmuir–Hinshelwood (L–H) kinetic model.

Table 1 shows the fitted kinetic parameters for photo-inactivation of *E. coli* in the TNC–ASP system from using different empirical models. Results showed that the Hom model was only applicable at the optimal TNC loading of 1.0 g/L, where the ROS volumetric rate was maximal (i.e. length of shoulder characteristic region is the shortest). Thus, the Hom model can only selectively reproduce the tailing characteristic region of the bacterial survivor curves found in this study. The $m$ value for the Hom model that accounted for the tailing characteristic was found to be $m=0.71$. This $m$-value suggested the presence of strong tailing for photo-inactivation activity of *E. coli* in the TNC–ASP system (Gyürék and Finch, 1998). It was also found that the Hom model with $m>1$ can only reproduce the shoulder region, but not the tailing. Because of the empirical nature of the Hom model, the $m>1$ actually suggested an increase in photo-inactivation reactivity with irradiation time. If the vitalistic assumption of bacterial population resistance distribution is valid, this actually signifies that the most resistant bacteria are killed first prior to the least resistant (Lambert and Johnston, 2000).

**Table 1**
Numerical evaluation for the fittingness of each empirical model on the inactivation kinetics of *E. coli* using TNC photocatalyst at a concentration of 1.0 g $L^{-1}$.

| *Empirical model* | *k* | $k_1$ | $k_2$ | $k_3$ | *m* | *n* | *x* | $N_0$ | *Correlation coefficient* $R^2$ |
|---|---|---|---|---|---|---|---|---|---|
| Hom | 0.1128 (L/g min) | – | – | – | 0.7114 | 1.1059 | – | – | 0.9891 |
| Hom-power | 0.3452 (L/g CFU) | | | | 0.8783 | 2.03 | 0.9191 | 7.15E+06 | 0.9907 |
| Modified hom | – | 3.2668 | 0.0333 | 2.7589 | – | – | – | – | 0.9959 |
| Rational | 0.9043 (L/g min CFU) | – | – | – | – | 0.861 | 1.0952 | 7.15E+06 | 0.9938 |
| Selleck | 0.9635 (L/g min) | – | – | – | – | 1.1526 | – | – | 0.8439 |

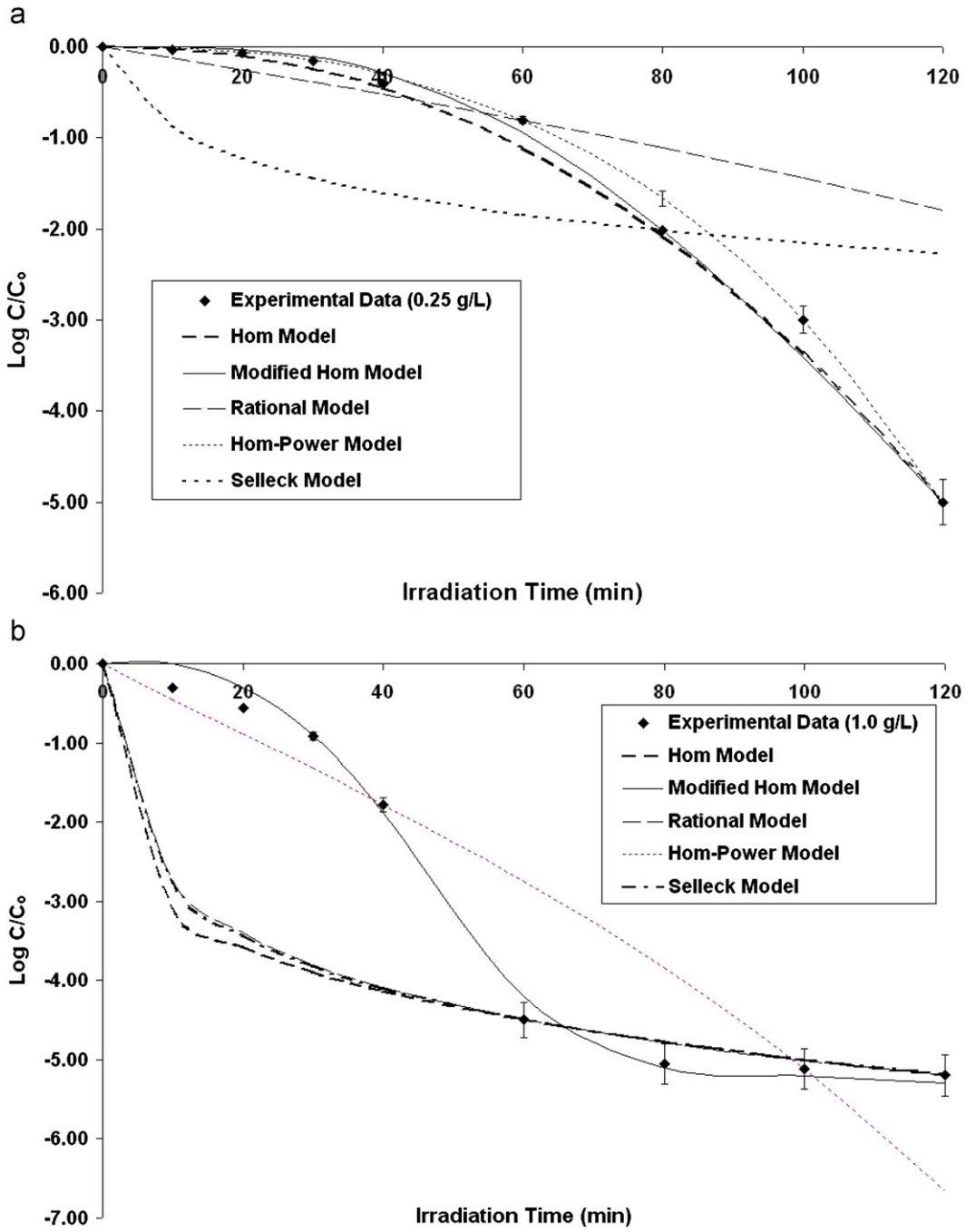


**Fig. 3.** Fitting of different empirical disinfection kinetic models for TNC loading at (a) 0.25 g $L^{-1}$ and (b) 1.0 g $L^{-1}$ respectively. The average initial *E. coli* concentration is $7 \times 10^6$ CFU $mL^{-1}$ and UV-A irradiation starts at $t=0$ min.

Thus, the empirical Hom model can only be used for experimental data analysis and comparison, rather than portraying any physical meaning for the photo-inactivation mechanisms of *E. coli*.

The experimental data obtained from using TNC loading of 1.0 g /L was also fitted with the Hom-Power law, Rational model and the modified Hom model. The Rational model was able to reproduce partial shoulder and tailing characteristic regions with a certain logarithmic limitation at $x=1.09$. This Rational model was found to provide a better fitting over the Hom-Power law as evidenced from the Pearson correlation coefficient $R^2$. Although the Hom-Power law functionalised on four kinetic parameters, its logarithmic nature has restricted the ability to simultaneously represent both the shoulder and tailing behaviours. In this instance, the smooth inflexion of bacterial survivor curves with shoulder, log-linear and tailing regions was confined to the elementary logarithmic inactivation curve (i.e. no tailing representation) when the Hom-Power law was used. This over-parameterization model also provided a null physical meaning for each kinetic parameter that represents the photo-inactivation mechanisms in the TNC–ASP system. Overall, the modified Hom model provided the best representation of photo-inactivation kinetics of *E. coli* in the TNC–ASP system. It was also found that the modified Hom model gives a more realistic mathematical expression as it represented all the bacterial inactivation regimes within the kinetics curve. Among all the empirical models, the Selleck model appeared to be the least favourable to represent the photo-inactivation action of TNC in this study. Fig. 3 compares the fittingness of five different empirical models under the TNC loadings of 0.25 and 1.0 g/L. From Fig. 3, it is seen that most of the empirical models were best fitted at TNC loading of 1.0 g/L than 0.25 g/L. This was found to be owing to the curvilinear nature of the curve at TNC loading of 0.25 g/L (shoulder and tailing regions not evident), where the fitting of higher parameterized empirical models were not appropriate. The fitting of the modified Hom model for different TNC loadings is shown in Fig. 4. With all these estimated kinetic parameters, the photo-inactivation activity in the ASP system using TNC can be compared with other photocatalytic inactivation systems.

### 3.3. Proposition and validation of photo-inactivation mechanistic model

Although the empirical models usually provide a better fitting for the experimental data, the mathematical nature of their relevant terms usually yields null physical meaning in representing the "*true*" inactivation behaviours. To elucidate the superiority of the mechanistic model in expressing the photo-inactivation action of TNC in the ASP system, a mechanistic model was applied for the experimental data found in this study.

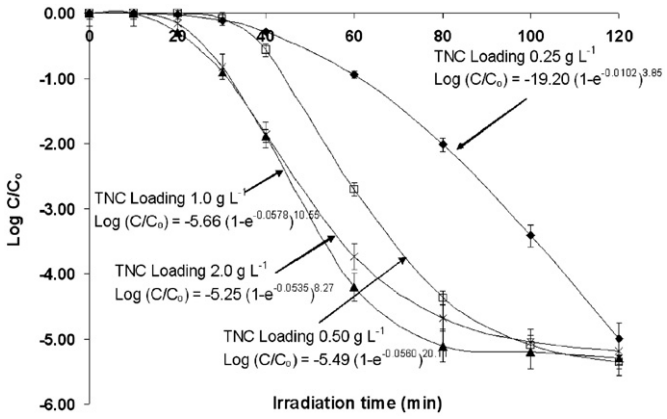


**Fig. 4.** Fitting of modified Hom empirical model to experimental data with different TNC loadings. The average initial *E. coli* density is $7\times10^6$ CFU mL$^{-1}$ and UVA irradiation starts at $t=0$ min.

In the mechanistic hypothesis, the disinfection mechanism is assumed to be a pure physicochemical phenomenon, and proceeds in a similar way as a chemical reaction (Lambert and Johnston, 2000). The classical CW model (Eq. (7)) is a typical example of the mechanistic model:

$$\frac{dN}{dt} = -k_o N \tag{7}$$

This basic CW equation dictates that the apparent exponential decay curves for bacterial survival ratio against irradiation time follows a similar decay mechanism to a chemical reaction, and is applicable under both phenomena. This can be visualised when Eq. (7) is mathematically integrated, where $N$ assumes to be the number of moles of reactant to yield the log-linear curve of a first order chemical reaction.

To fit the kinetics data from the photo-inactivation reaction in TNC–ASP system using a mechanistic model, however, one needs to have idealistic rationales to account for the shoulder and tailing characteristic regions in the bacterial survivor curve (Fig. 2a). The presence of a shoulder region can be justified mechanistically via the single-hit multiple targets or a series phenomenon event (Gyürék and Finch, 1998). Under this approach, the damage on the bacterial cell is viewed as cumulative rather than instantly lethal. This dictates that a large number of critical molecules need to be denatured prior to the inactivation of the cell (Gyürék and Finch, 1998). Severin et al. (1984) proposed that the cumulative inactivation of a single organism can be collectively represented by a series of integer steps. In this postulation model, the inactivation steps are assumed to be passed on an organism from one level to another in a first order reaction with respect to the TNC loading applied until a finite number of damaged (*dam*) events are achieved. A bacterium that accumulates less than the postulated number of damaged steps is considered to survive the photo-inactivation reaction. To validate this postulation model, however, sufficient loadings have to be ensured to ascertain that the volumetric ROS generation rate is far exceeds the bacterial growth rate.

Many researchers regard that the existence of a tailing characteristic region is owing to the presence of microbial subpopulation resistant to disinfection. Najm (2006) supported a similar proposition that the tailing behaviour is due to the intrinsic distribution of bacterial resistance, which makes the bacteria more resistant, adapted and inaccessible to disinfection. To date, no justifiable explanation is proposed to account for the occurrence of tailing behaviour during water disinfection treatment with well-mixed conditions and equally resistant, genetically cloned bacterial populations. Some studies discussed that the tailing characteristic in the bacteria survivor curves is a result of gradual decline in the rate of inactivation and thus, the total inactivation is only achievable after certain irradiation time (Najm, 2006).

In this study, we found that TNC loadings of higher than 1.0 g/L resulted in significant prolongation of irradiation time to achieve a 5-log reduction level. At an extended irradiation time of 360 min (data not shown), the highest bacterial inactivation level achieved was only a 4.5 log reduction. This finding did not only conform to our earlier hypothesis for total inactivation after certain irradiation time for tailing, but also confirmed the impacts of TNC loadings and reactor dimensions (i.e. annulus width) (Shiraishi et al., 1999). The current annulus width for the ASP system is 5 cm. This means that the constant UVA intensity used can easily penetrate through the low TNC loadings to provide full illumination for catalyst activation and even to the *E. coli* adhered

on the internal surfaces of the ASP (Hong and Otaki, 2003). At elevated TNC loadings, we found a decreasing rate in bacterial inactivation level coupled with the existence of tailing behaviours. This was probably due to the fact that increasing TNC loadings reduce the UVA penetration through reaction suspension, and thus are only able to provide partial illumination for catalyst activation up to the internal ASP surfaces. A reduction in the current annulus width is expected to yield a higher bacterial photo-inactivation rate with no tailing characteristic. At the constant annulus width, however, an increase in TNC loadings can be contemplated by using a higher UVA lamp output which results in a stronger penetrative energy through the reaction suspension. This can be the solution when real water/wastewater is encountered with increasing mixing effect of catalyst particles, turbidity, inorganic ions and other water quality-related parameters (Rincón and Pulgarin, 2003). So far, there is no single postulation that can ideally account for the tailing in water disinfection. All these propositions were acceptable under theoretical explanation for the observed tailing behaviour.

Lambert and Johnston (2000) stated that in the formulation of mechanistic models that take into account non-linearity in inactivation behaviours, an intermediate population stage was suggested having different disinfection rates for each microbial state. In this study, two different microbial states for the number of damaged bacteria and un-damaged bacteria (i.e. $C_{dam}+C_{undam}$) were used to account for the non-linearity. Owing to the adsorptive nature of photocatalytic reaction, a L–H type of mechanistic kinetic model was applied (Eqs. (8) and (9)) (Marugán et al., 2008). Since the TNC loading was found to be a non-limiting reactant of DO at its optimal concentration, we proposed two different kinetic expressions for each microbial state that take into account the DO concentration level change in the ASP system.

$$\frac{dC_{undam}}{dt} = \frac{-k_{undam}K_{undam}C^{\alpha}_{undam}}{1+K_{undam}C^{\alpha}_{undam}+K_{dam}C^{\alpha}_{dam}+K_{O_2}[\mathrm{DO}/\mathrm{DO}_o]^{\alpha}(C^{\alpha}_{undam}+C^{\alpha}_{dam})} \quad (8a)$$

$$\frac{dC_{undam}}{dt} = \frac{-k_{undam}K_{undam}C^{\alpha}_{undam}}{1+K_{undam}C^{\alpha}_{undam}+K_{dam}C^{\alpha}_{dam}} \quad (8b)$$

$$\frac{dC_{dam}}{dt} = \frac{k_{undam}K_{undam}C^{\alpha}_{undam}-k_{dam}K_{dam}C^{\alpha}_{dam}}{1+K_{undam}C^{\alpha}_{undam}+K_{dam}C^{\alpha}_{dam}+K_{O_2}[\mathrm{DO}/\mathrm{DO}_O]^{\alpha}(C^{\alpha}_{undam}+C^{\alpha}_{dam})} \quad (9a)$$

$$\frac{dC_{dam}}{dt} = \frac{k_{undam}K_{undam}C^{\alpha}_{undam}-k_{dam}K_{dam}C^{\alpha}_{dam}}{1+K_{undam}C^{\alpha}_{undam}+K_{dam}C^{\alpha}_{dam}} \quad (9b)$$

where $k_i$ is the true log-linear deactivation rate constant for *E. coli*. The pseudo-interaction constant, $K_i$, represents the surface interaction between TNC and *E. coli*. In the conventional L–H model for chemical reaction, $K_i$ actually represents the strict adsorption of reactants onto the active sites of the catalyst. Due to the significant size differences between *E. coli* and TNC, this term is better visualised as an interaction term that accounts for the shoulder appearance than the usual strict adsorption phenomenon. The inhibition coefficient, $\alpha$, is a power-law expression that accounts for the tailing behaviour in the inactivation curve. Although this inhibition coefficient can be fixed at $\alpha=1$, where the $K_i$ can be expressed in terms of apparent $K_i'$, such simplification should be avoided to prevent the under-representativeness of true tailing behaviours.

The new mechanistic models show that two different expressions were proposed for each microbial state ($C_{dam}$ and $C_{undam}$). This was found to be in agreement with the observed DO concentration profile at the optimal TNC loading. We found that the rapid ROS generation rate resulted in a non-limiting condition of DO reactant. It should be emphasised that DO is one of the basic reactants in photocatalysis, and insufficient DO can result in a limiting reaction condition. Thus, two different expressions were proposed for each microbial state in order to visualise the importance of DO as a limiting reactant at $\mathrm{TNC}<\mathrm{TNC}_{optimal}$ (Eqs. (8a) and (9a)) and non-limiting at $\mathrm{TNC}=\mathrm{TNC}_{optimal}$ (Eqs. (8b) and (9b)). The $K_{O_2}$ term is evaluated independently via the measured DO isotherms as shown in Fig. 2b. So far, there are limited investigations reported in the literature to correlate the effect of photocatalyst loading to its corresponding DO level (Cho et al., 2004). This correlation can be explained by the unique long

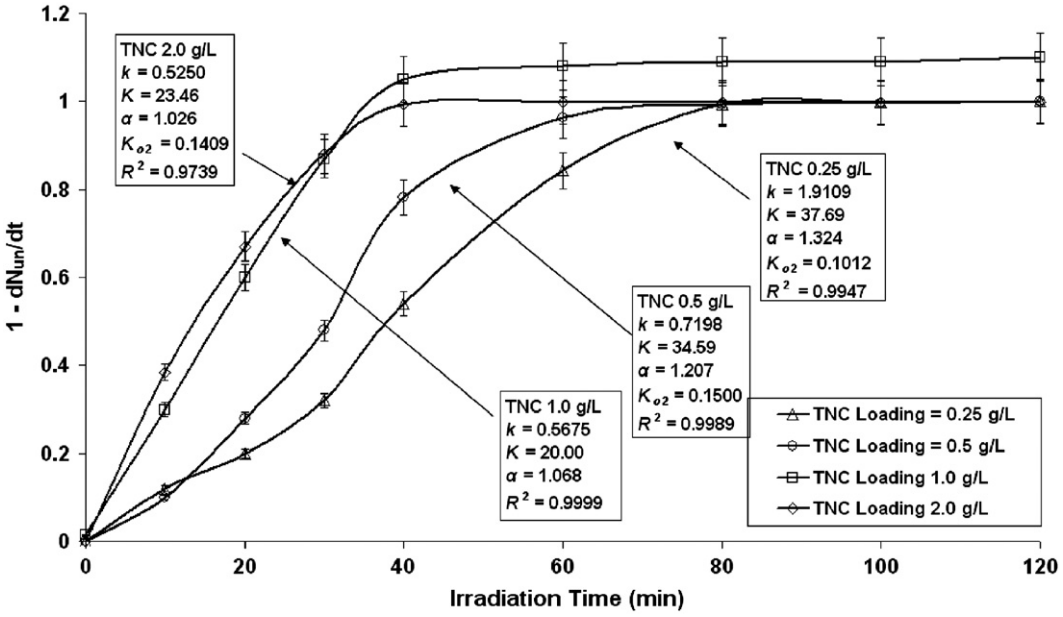


**Fig. 5.** Fitting of a mechanistic kinetic model to experimental data of photocatalytic inactivation of average *E. coli* density of $7\times10^6$ CFU mL$^{-1}$. The UV-A irradiation starts at $t=0$ min.

fibril TNC morphology that is dissimilar to the commercial Degussa P25 $TiO_2$ photocatalyst. The Degussa P25 $TiO_2$ demonstrates certain mass transfer limitations in terms of long diffusional paths for organic, microbial contaminants, light photon and DO, respectively (Chen et al., 1995). The thin titanate fibril of 40–100 nm with anatase $TiO_2$ crystals of 10–20 nm was able to shorten the diffusional path and thus, promote rapid rates of DO evolution and surface reaction in the TNC–ASP system (Chong et al., 2009b).

One of the disadvantages of the proposed mechanistic models is that they require prior knowledge on the optimal photocatalyst loading. To evaluate these models, some assumptions have been made to prevent over-parameterization. Marugán et al. (2008) stated that the rate constant should equate to; $k_{dam}=k_{undam}=k$ and similarly the surface interaction constants, $K_{dam}=K_{undam}=K$. These reduce the proposed models to

$$\frac{dC_{undam}}{dt}=\frac{-kKC_{undam}^{\alpha}}{1+K(C_{undam}^{\alpha}+C_{dam}^{\alpha})+K_{O_2}[\mathrm{DO}/\mathrm{DO}_o]^{\alpha}(C_{undam}^{\alpha}+C_{dam}^{\alpha})} \tag{10a}$$

$$\frac{dC_{undam}}{dt}=\frac{-kKC_{undam}^{\alpha}}{1+K(C_{undam}^{\alpha}+C_{dam}^{\alpha})} \tag{10b}$$

$$\frac{dC_{dam}}{dt}=\frac{kK(C_{undam}^{\alpha}-C_{dam}^{\alpha})}{1+K(C_{undam}^{\alpha}+C_{dam}^{\alpha})+K_{O_2}[\mathrm{DO}/\mathrm{DO}_o]^{\alpha}(C_{undam}^{\alpha}+C_{dam}^{\alpha})} \tag{11a}$$

$$\frac{dC_{dam}}{dt}=\frac{kK(C_{undam}^{\alpha}-C_{dam}^{\alpha})}{1+K(C_{undam}^{\alpha}+C_{dam}^{\alpha})} \tag{11b}$$

Fig. 5 shows the fitting of experimental data using the proposed L–H mechanistic photo-inactivation models. These models gave a higher degree of fittingness. One problem, which was encountered during the parameter estimation is that the oxygen-interaction term, $K_{O_2}$, needs to be first evaluated and the DO term was normalised $[DO/DO_o]$ to achieve dimensional homogeneity with other denominator terms. The physical meaning of DO limiting term, $K_{O_2}[\mathrm{DO}/\mathrm{DO}_o]^{\alpha}(C_{undam}{}^{\alpha}+C_{dam}{}^{\alpha})$, actually signifies the presence of competition between dissolved oxygen, undamaged bacteria and bacterial lysis products for surface active

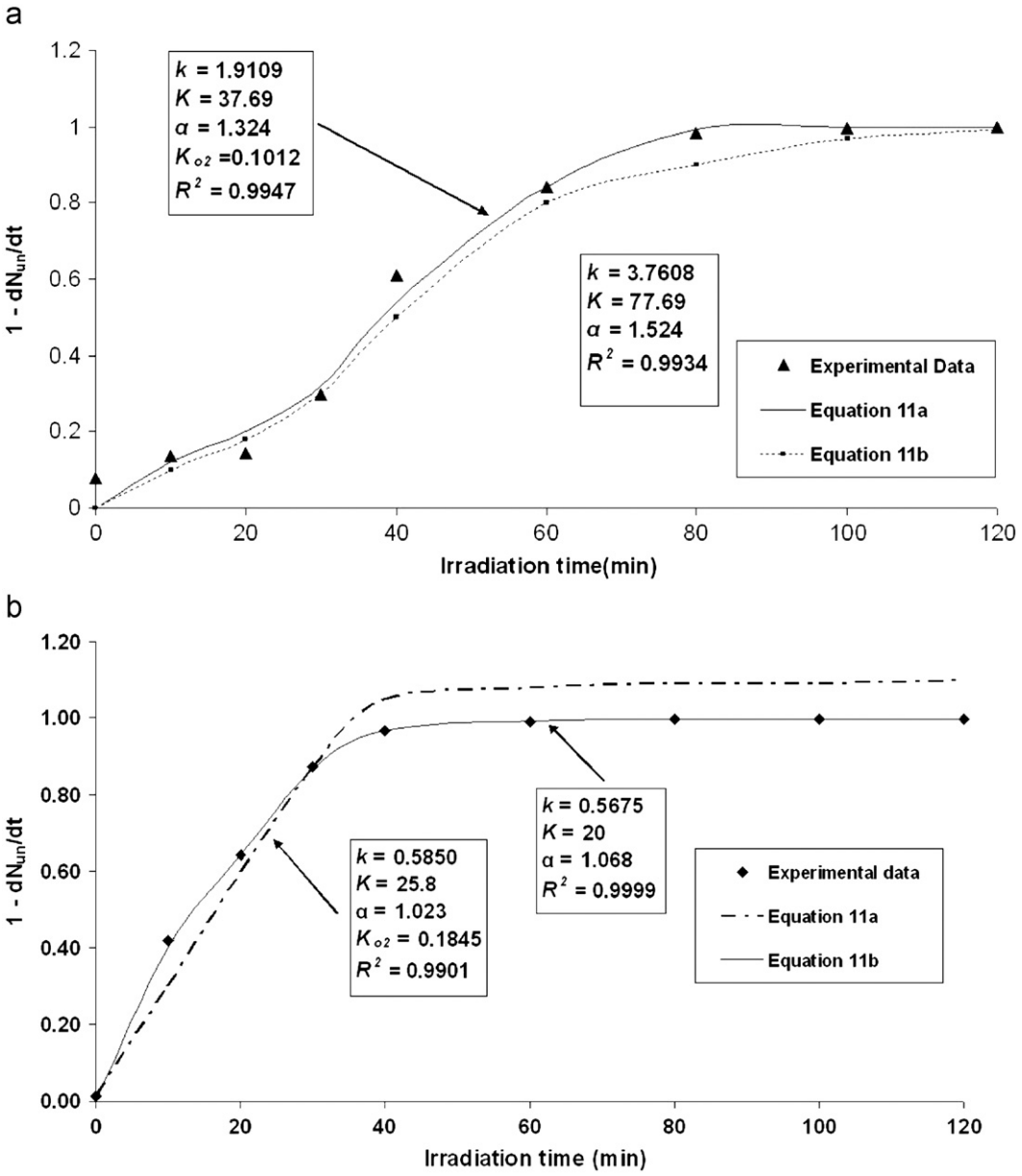


**Fig. 6.** Cross validation for the proposed mechanistic models at TNC loadings of (a) 1.0 g $L^{-1}$ and (b) 0.25 g $L^{-1}$. The average *E. coli* density is $7\times10^6$ CFU $mL^{-1}$ and the UV-A irradiation starts at $t=0$ min.

sites. At an increasing $K$-value, the length of the shoulder characteristic region was increased to enable interaction and longer reaction time for prime lethality events to occur. In addition, it should be noted from Fig. 5 that the tendency of tailing was represented when $\alpha$ was greater than unity. Fig. 5 shows that all the $\alpha$ values are greater than unity, indicating that the reaction order is higher than unity with respect to the bacterial numbers. This might be owing to the competition between un-damaged bacteria and breakdown products for active sites on the surface of the catalysts, which directly resulted in a higher reaction order for the tailing characteristic region. Fig. 6a shows the cross validation for the proposed models at optimal TNC loading, where the applicability and validity of Eq. (11a) was tested. A lower $R_2$ value for the experimental data was observed when using the DO limiting models. When the experimental data for non-optimal TNC loading was tested on the DO non-limiting models (Eq. (11b)), the surface-interaction constant ($K$) yielded a significantly higher value than those reported in Fig. 5. It was understood that the surface-interaction constants take the $K_{O_2}[DO/DO_o]^{\alpha}(C_{undam}{}^{\alpha}+C_{dam}{}^{\alpha})$ into account by integrating the effects into a singular apparent constant of $K'$ (i.e. $K'=K.K_{O_2}[DO/DO_o]^{\alpha}(C_{undam}{}^{\alpha}+C_{dam}{}^{\alpha})$). All these have proven the rationale of correlating the effect of DO on the photo-inactivation action of TNC in the ASP system. Thus, the L–H models were considered as a more realistic approach to represent the bacterial photo-inactivation activity in the TNC–ASP system, in terms of its fittingness, physical meaning of each term and the practical integration of DO as a limiting reactant under non-optimal TNC loadings.

### 3.4. Conclusion

Here, we have come to a few conclusive points from the experimental study Hereon photo-inactivation of a sewage isolated *E. coli* strain (ATCC 11775) in the TNC–ASP system. At the optimal TNC loading, DO was found to be a non-limiting reactant during the photo-inactivation reaction on *E. coli*. The rapid rejuvenation in DO concentration level under optimal TNC loading was deduced to be owing to its thin fibril morphology that shortens the diffusional path for DO, and subsequently promotes rapid DO evolution rate and surface reaction. However, at other TNC loadings DO appeared to be a limiting reactant in the photo-inactivation reaction of *E. coli*.

The photo-inactivation kinetics and mechanisms of *E. coli* in the TNC–ASP system were evaluated and validated using different empirical bacterial inactivation models. Since the bacterial inactivation profiles are highly non-linear, empirical models with at least three physical parameters were found to adequately represent the experimental data. The empirical models of modified-Hom, Rational and Hom-Power can adequately represent the photo-inactivation activity of *E. coli* within the TNC–ASP system. However, it was found that the logarithmic nature of Rational and Hom-Power models restricted the curve inflexion for simultaneous representation of shoulder and tailing behaviours. In this instance, the modified Hom model was found to be the best empirical model for describing the photo-inactivation action of TNC on *E. coli* in the ASP system. With all these estimated kinetic parameters, the photo-inactivation activity in the ASP system using TNC can be compared with other photocatalytic inactivation systems.

The L–H mechanistic models with three parameters of; (1) log-linear reaction rate ($k$), (2) surface-interaction constant ($K$) and (3) inhibition/tailing coefficient ($\alpha$) were adopted to give a better kinetic representation and physical description for the photo-inactivation action on *E. coli* in the TNC–ASP system. These L–H models were further correlated to the DO concentration profiles during the photo-inactivation reaction on *E. coli* under two different TNC loading conditions: (1) sub-optimal and (2) optimal conditions. At the sub-optimal TNC loadings, DO acts as a limiting reactant and its absence causes a pertinent effect to the bacteria inactivation rate; whereas DO was found to be a non-limiting reactant under the optimal TNC loading. Experimental validations on the proposed DO correlated L–H models under both sub-optimal and optimal TNC loadings were examined to confirm the observed DO relationship. It is anticipated that such mechanistic models can be applicable to simulate the photo-inactivation kinetics of bacteria under different types of photocatalyst and water quality matrixes.

## Acknowledgement

The authors would like to thank Mr Philip Adcock for his valuable discussion and feedback during the initial planning stage of this study, and Associate Professor Huaiyong Zhu for providing the TNC samples. This work was funded by the Australian Research Council Linkage Grant (LP0562153) and the Australian Water Quality Centre, SA Water Corporation through the Water Environmental Biotechnology Laboratory (WEBL) at the University of Adelaide.

## References

Anotai, J., 1996. Effect of Calcium Ions on Chemistry and Disinfection Efficiency of Free Chlorine at pH 10. Ph.D. Dissertation. Drexel University, Philadelphia, Pa.

Benabbou, A.K., Derriche, Z., Felix, C., Lejeune, P., Guillard, C., 2007. Photocatalytic inactivation of Escherichia coli: Effect of concentration of $TiO_2$ and micro-organism, nature, and intensity of UV irradiation. Appl. Catal. B: Environ. 76, 257–263.

Bull, R.J., Gerba, C.P., Trussell, R.R., 1990. Evaluation of the health risks associated with disinfection. Crit. Rev. Environ. Control 20, 77–114.

Burch, J., Thomas, K.E., 1998. An Overview of Water Disinfection in Developing Countries and the Potential for Solar Thermal Water Pasteurization. National Renewable Energy Laboratory NREL/TP-550-23110.

Carter, J.T., Rice, E.W., Buchburger, S.G., Lee, Y., 2000. Relationships between levels of heterotrophic bacteria and water quality parameters in a drinking water distribution system. Water Res. 34 (5), 1495–1502.

Chen, H.Y., Zahraa, O., Bouchy, M., Thomas, F., Bottero, J.Y., 1995. Adsorption properties of $TiO_2$ related to the photocatalytic degradation of organic contaminants in water. J. Photochem. Photobiol. A: Chem. 85, 179–186.

Cho, M., Chung, H., Yoon, J., 2003. Disinfection of water containing natural organic matter by using ozone-initiated radical reactions. Appl. Environ. Microbiol. 69 (4), 2284–2291.

Cho, M., Chung, H., Choi, W., Yoon, J., 2004. Linear correlation between inactivation of *E. coli* and OH radical concentration in $TiO_2$ photocatalytic disinfection. Water Res. 38, 1069–1077.

Chong, M.N., Vimonses, V., Lei, S., Jin, B., Chow, C., Saint, C., 2009a. Synthesis and characterisation of novel titania impregnated kaolinite nano-photocatalyst. Micropor. Mesopor. Mater. 117 (1), 233–242.

Chong, M.N., Jin, B., Zhu, H.Y., Chow, C.W.K., Saint, C., 2009b. Application of H-titanate nanofibers for degradation of congo red in an annular slurry photoreactor. Chem. Eng. J. 150 (1), 49–54.

Chong, M.N., Jin, B., Chow, C.W.K., Saint, C., 2010a. Recent developments in photocatalytic water treatment technology: a review. Water Res. 44 (10), 2997–3027.

Chong, M.N., Jin, B., Zhu, H., Saint, C., 2010b. Bacterial inactivation kinetics, regrowth and synergistic competition in a photocatalytic disinfection system using anatase titanate nanofiber catalyst. J. Photochem. Photobiol. A: Chem. 214, 1–9.

Chong, M.N., Zhu, H.Y., Jin, B., 2010c. Response surface optimization of photocatalytic process for degradation of congo red using H-titanate nanofiber catalyst. Chem. Eng. J. 156, 278–285.

Chong, M.N., Jin, B., Saint, C.P., 2011. Bacterial inactivation kinetics of a photo-disinfection system using novel titania-impregnated kaolinite photocatalyst. Chem. Eng. J. 171, 16–23.

Coleman, H.M., Marquis, C.P., Scott, J.A., Chin, S.S., Amal, R., 2005. Bactericidal effects of titanium dioxide-based photocatalysts. Chem. Eng. J. 113, 55–63.

Dalrymple, O.K., Stefanakos, E., Trotz, M.A., Goswami, D.Y., 2010. A review of the mechanism and modelling of photocatalytic disinfection. Appl. Catal. B: Environ. 98, 27–38.

Dunlop, P.S.M., Byrne, J.A., Manga, N., Eggins, B.R., 2002. The photocatalytic removal of bacterial pollutants from drinking water. J. Photochem. Photobiol. A: Chem. 148, 355–363.

Foster, H.A., Ditta, I.B., Varghese, S., Steele, A., 2011. Photocatalytic disinfection using titanium dioxide: spectrum and mechanism of antimicrobial activity. Appl. Microbiol. Biotechnol. 90 (6), 1847–1868.

Gamage, J., Zhang, Z., 2010. Applications of photocatalytic disinfection. Int. J. Photoenergy 2010 (Article ID 764870), 11–21.

Gyürék, L.L., Finch, G.R., 1998. Modelling water treatment chemical disinfection kinetics. J. Environ. Eng. 124 (9), 783–793.

Hom, L.W., 1972. Kinetics of chlorine disinfection in an ecosystem. J. Sanit. Eng. Div. 98 (1), 183–194.

Hong, J., Otaki, M., 2003. Effects of photocatalysis on biological decolorization reactor and biological activity of isolated photosynthetic bacteria. J. Bio. Bioeng. 96 (3), 298–303.

Ibánez, J.A., Litter, M.I., Pizarro, R.A., 2003. Photocatalytic bactericidal effect of $TiO_2$ on Enterobacter cloacae: comparative study with other gram (−) bacteria. J. Photochem. Photobiol. A: Chem. 157, 81–85.

Lambert, R.J.W., Johnston, M.D., Simons, E.A., 1999. A kinetic study of the effect of hydrogen peroxide and peracetic acid against *Staphylococcus aureus* and *Pseudomonas aeruginosa* using the Bioscreen disinfection method. J. Appl. Microbiol. 87, 782–786.

Lambert, R.J.W., Johnston, M.D., 2000. Disinfection kinetics: a new hypothesis and model for the tailing of log-survivor/time curves. J. Appl. Microbiol. 88, 907–913.

Maness, P.C., Smolinski, S., Blake, D.M., Huang, Z., Wolfrum, E.J., Jacoby, W.A., 1999. Bactericidal activity of photocatalytic $TiO_2$ reaction: toward an understanding of its killing. Appl. Environ. Microbiol. 65 (9), 4094–4098.

Marugán, J., Grieken, R.V., Sordo, C., Cruz, C., 2008. Kinetics of the photocatalytic disinfection of Escherichia coli suspensions. Appl. Catal. B: Environ. 82, 27–36.

Matsunaga, T., Tomodam, R., Nakajima, T., Wake, H., 1985. Photochemical sterilization of microbial cells by semiconductor powders. FEMS Microbiology Letters 29, 211–214.

McCullagh, C., Robertson, J.M.C., Bahnemann, D.W., Robertson, P.K.J., 2006. The application of $TiO_2$ photocatalysis for disinfection of water contaminated with pathogenic micro-organisms: a review. Res. Chem. Intermediat. 33, 359–375.

Najm, I., 2006. Formation of hydrazine as a chloramine by-product. J. Am. Water Works Assoc. 98, 93–101.

Rincón, A.G., Pulgarin, C., 2003. Photocatalytic inactivation of *E. coli*: effect of continuous-intermittent) light intensity and of (suspended-fixed) $TiO_2$ concentration. Appl. Catal. B: Environ. 44, 263–284.

Rincón, A.G., Pulgarin, C., 2004. Effect of pH, inorganic ions, organic matter and $H_2O_2$ on *E. coli* K12 photocatalytic inactivation by $TiO_2$: implications in solar water disinfection. Appl. Catal. B: Environ. 51, 283–302.

Rincón, A.G., Pulgarin, C., 2005. Use of coaxial photocatalytic reactor (CAPHORE) in the $TiO_2$ photo-assisted treatment of mixed *E. coli* and *Bacillus* sp. and bacterial community present in wastewater. Catal. Today 101, 331–344.

Rincón, A.G., Pulgarin, C., 2006. Comparative evaluation of $Fe^{3+}$ and $TiO_2$ photo-assisted processes in solar photocatalytic disinfection of water. Appl. Catal. B: Environ. 63, 222–231.

Severin, B.F., Suidan, M.T., Engelbrecht, R.S., 1984. Series-event kinetic model for chemical disinfection. J. Environ. Eng. ASCE 110 (2), 430–439.

Shiraishi, F., Toyoda, K., Fukinbara, S., Obuchi, E., Nakano, K., 1999. Photolytic and photocatalytic treatment of an aqueous solution containing microbial cells and organic compounds in an annular-flow reactor. Chem. Eng. Sci. 54, 1547–1552.

Smith, H.V., Rose, J.B., 1998. Waterborne cryptosporidiosis: current status. Parasitol. Today 14 (1), 14–22.

Sun, D.D., Tay, J.H., Tan, K.M., 2003. Photocatalytic degradation of E.coliform in water. Water Res. 37, 3452–3462.

US EPA, 2001. Stage 1 Disinfectants and Disinfection Byproducts Rule. United States Environmental Protection Agency EPA 816-F-01-014, June 2001.

Vidal, A., Diaz, A.I., El Hraiki, A., Romero, M., Muguruza, I., Senhaji, F., Gonzalez, J., 1999. Solar photocatalysis for detoxification and disinfection of contaminated water: pilot plant studies. Catal. Today 54 (2), 283–290.

Vogt, C., Regli, S., 1981. Controlling THM while attaining disinfection. J. Am. Water Works Assoc. 73 (1), 33–40.

Watts, R.J., Kong, S., Orr, M.P., Miller, G.C., Henry, B.E., 1994. Photocatalytic inactivation of coliform bacteria and viruses in secondary wastewater effluent. Water Res. 29 (1), 95–100.

Wolfrum, E.J., Huang, J., Blake, D.M., Maness, P.C., Huang, Z., Fiest, J., 2002. Photocatalytic oxidation of bacteria, bacterial and fungal spores, and model biofilm components to carbon dioxide on titanium dioxide-coated surfaces. Environ. Sci. Technol. 36, 3412–3419.

WHO, 1997. Guidelines for drinking water quality. Surveillance and Control of Community Supplies, vol. 3. World Health Organisation, Geneva, Switzerland.

Zhu, H., Gao, X., Lan, Y., Song, D., Xi, Y., Zhao, J., 2004. Hydrogen titanate nanofibers covered with anatase nanocrystals: a delicate structure achieved by the wet chemistry reaction of the titanate nanofibers. J. Am. Chem. Soc. 126 (27), 8380–8381.

Zhu, H.Y., Lan, Y., Gao, X.P., Ringer, S.P., Zheng, Z.F., Song, D.Y., Zhao, J.C., 2005. Phase transition between nanostructures of titanate and titanium dioxides via simple wet-chemical reactions. J. Am. Chem. Soc. 127, 6730–6736.